



PERGAMON

International Journal of Plasticity 19 (2003) 235–251

INTERNATIONAL JOURNAL OF
Plasticity

www.elsevier.com/locate/ijplas

Finite deformation analysis of mechanism-based strain gradient plasticity: torsion and crack tip field

K.C. Hwang^a, H. Jiang^a, Y. Huang^{b,*}, H. Gao^c

^a*Failure Mechanics Laboratory, Department of Engineering Mechanics, Tsinghua University,
Beijing 100084, People's Republic of China*

^b*Department of Mechanical and Industrial Engineering, University of Illinois, Urbana, IL 61801, USA*

^c*Division of Mechanics and Computation, Stanford University, Palo Alto, CA 94305, USA*

Received in final revised form 27 June 2001

Abstract

A finite deformation theory of mechanism-based strain gradient (MSG) plasticity is developed in this paper based on the Taylor dislocation model. The theory ensures the proper decomposition of deformation in order to exclude the volumetric deformation from the strain gradient tensor since the latter represents the density of geometrically necessary dislocations. The solution for a thin cylinder under large torsion is obtained. The numerical method is used to investigate the finite deformation crack tip field in MSG plasticity. It is established that the stress level around a crack tip in MSG plasticity is significantly higher than its counterpart (i.e. HRR field) in classical plasticity. © 2002 Elsevier Science Ltd. All rights reserved.

Keywords: Finite deformation; Strain gradient plasticity; Torsion; Fracture

1. Introduction

The size dependence observed in recent experiments at the micron and submicron scales (e.g. Fleck et al., 1994; Lloyd, 1994; McElhane et al., 1998; Stolken and Evans, 1988) and in direct dislocation simulations (Cleveringa et al., 1997, 1998, 1999a,b; 2000; Shizawa and Zbib, 1999; Needleman, 2000; Zbib and de la Rubia, 2001) have motivated the development of strain gradient plasticity theories based on the concept of geometrically necessary dislocation (Nye, 1953; Cottrell, 1964; Ashby, 1970; Arsenlis and Parks, 1999; Gurtin, 2000). The strain gradient serves

* Corresponding author. Tel.: +1-217-265-5072; fax: +1-217-244-6534.

E-mail address: huang9@uiuc.edu (Y. Huang).

either as an independent measure of deformation besides the strain (e.g. Fleck and Hutchinson, 1993, 1997; Shu, 1998; Gao et al., 1999; Shu and Fleck, 1999; Huang et al., 2000a,b; Shu and Barlow, 2000; Gurtin, 2001), or as an internal variable to increase the plastic work hardening modulus (e.g. Nilsson, 1998; Acharya and Basani, 2000; Acharya and Beaudoin, 2000; Chen and Wang, 2000; Dai and Parks, 2001; Meissonnier et al., 2001). There are also early works on strain gradient plasticity that were proposed in order to avoid a spurious solution for the localized zone and an excessive mesh dependence in classical plasticity (e.g. Aifantis, 1984, 1992; Lasry and Belytschko, 1988; Zbib and Aifantis, 1988; Muhlhaus and Aifantis, 1991; de Borst and Muhlhaus, 1991, 1992; Sluys et al., 1993).

Since the aforementioned micron and submicron scale experiments involve large deformation, Hwang et al. (2001) generalized Fleck and Hutchinson's (1997) and Gao et al.'s (1999) strain gradient plasticity theories from infinitesimal to finite deformation. The equilibrium equations and boundary conditions are established in the current configuration, while the constitutive relations are obtained by nominal generalization from the corresponding infinitesimal deformation theories. The infinitesimal strain ε_{ij} and its gradient $\varepsilon_{ij,k}$ are replaced by the Green–Lagrange strain E_{IJ} and the corresponding gradient in the reference configuration, $E_{IJ,K}$, respectively. Such a nominal generalization, however, does not always ensure the appropriate decomposition of deformation into the volumetric and deviatoric parts. For example, ε_{kk} is the volumetric strain in infinitesimal deformation, but its nominal generalization E_{KK} does not represent the volumetric strain in finite deformation. Instead, only the determinant $J = \det(\mathbf{F})$ of the deformation gradient $\mathbf{F} = \frac{\partial \mathbf{x}}{\partial \mathbf{X}}$ represents the volume change in finite deformation, where \mathbf{x} and \mathbf{X} denote the coordinates of a material point in the current and reference configurations, respectively.

The purpose of this paper is to develop a finite deformation strain gradient plasticity theory that ensures the proper decomposition of volumetric and deviatoric deformation. It is a generalization of a classical finite deformation plasticity theory in Section 2 that excludes the volumetric deformation. We focus on the finite deformation theory of mechanism-based strain gradient plasticity (Gao et al., 1999; Huang et al., 2000a,b), though the approach can also be applied to Fleck and Hutchinson's (1997) strain gradient plasticity theory. We then present the analytical solution for a thin cylinder under torsion, and numerical study of the crack tip field.

2. A finite deformation theory of classical plasticity

We first present a finite deformation theory of classical plasticity that excludes the volumetric deformation. Let \mathbf{X} and \mathbf{x} denote the coordinates of a material point in the reference (undeformed) and current (deformed) configurations, respectively. The deformation gradient $\mathbf{F} = \frac{\partial \mathbf{x}}{\partial \mathbf{X}}$ can be expressed in terms of the principal stretches λ_1 , λ_2 and λ_3 as

$$\mathbf{F} = \lambda_1 n_1 \mathbf{N}_I + \lambda_2 n_2 \mathbf{N}_{II} + \lambda_3 n_3 \mathbf{N}_{III}, \quad (1)$$

where n_1, n_2, n_3 and $\mathbf{N}_I, \mathbf{N}_{II}, \mathbf{N}_{III}$ are the principal stretch directions in the current and reference configurations, respectively. The volumetric deformation is characterized by the determinant of \mathbf{F} ,

$$J = \det(\mathbf{F}) = \lambda_1 \lambda_2 \lambda_3. \tag{2}$$

The right and left Cauchy–Green strain tensors \mathbf{C} and \mathbf{B} and the Green strain tensor \mathbf{E} are defined by

$$\mathbf{C} = \mathbf{F}^T \cdot \mathbf{F}, \quad \mathbf{B} = \mathbf{F} \cdot \mathbf{F}^T, \quad \mathbf{E} = \frac{1}{2}(\mathbf{C} - \mathbf{1}), \tag{3}$$

where $\mathbf{1}$ is the second-order identity tensor.

In order to exclude the volumetric deformation from \mathbf{F} , we define a modified deformation gradient

$$\bar{\mathbf{F}} = J^{-\frac{1}{3}} \mathbf{F}, \tag{4}$$

which has no volumetric deformation since $(\bar{\mathbf{F}}) = 1$. The isochoric right and left Cauchy–Green strain tensors, $\bar{\mathbf{C}}$ and $\bar{\mathbf{B}}$, and the isochoric Green strain tensor $\bar{\mathbf{E}}$, which all exclude the volumetric deformation, can be defined similar to (3) via $\bar{\mathbf{F}}$ by

$$\bar{\mathbf{C}} = \bar{\mathbf{F}}^T \cdot \bar{\mathbf{F}}, \quad \bar{\mathbf{B}} = \bar{\mathbf{F}} \cdot \bar{\mathbf{F}}^T, \quad \bar{\mathbf{E}} = \frac{1}{2}(\bar{\mathbf{C}} - \mathbf{1}). \tag{5}$$

It can be shown that $\bar{\mathbf{E}}$ degenerates to deviatoric strain tensor for infinitesimal deformation. The invariants of $\bar{\mathbf{C}}$ and $\bar{\mathbf{B}}$ are

$$\bar{I}_1 = I(\bar{\mathbf{C}}) = I(\bar{\mathbf{B}}) = (\lambda_1 \lambda_2 \lambda_3)^{-\frac{2}{3}} (\lambda_1^2 + \lambda_2^2 + \lambda_3^2), \tag{6}$$

$$\bar{I}_2 = II(\bar{\mathbf{C}}) = II(\bar{\mathbf{B}}) = (\lambda_1 \lambda_2 \lambda_3)^{\frac{2}{3}} (\lambda_1^{-2} + \lambda_2^{-2} + \lambda_3^{-2}), \tag{7}$$

and $III(\bar{\mathbf{C}}) = III(\bar{\mathbf{B}}) = 1$. The effective strain is defined by

$$\varepsilon^2 = \frac{2}{3} \bar{\mathbf{E}} : \bar{\mathbf{E}} = \frac{1}{6} (\bar{I}_1^2 - 2\bar{I}_1 - 2\bar{I}_2) + \frac{1}{2}, \tag{8}$$

which degenerates to the von Mises effective strain for infinitesimal deformation.

For a deformation theory of plasticity, the strain energy density function U (per unit volume in the reference configuration) of an isotropic solid generally takes the form

$$U = U(J, \bar{I}_1, \bar{I}_2) = U^V(J) + U^D(\varepsilon) \tag{9}$$

where U^V and U^D are the strain energy densities for the volumetric and deviatoric deformation, respectively. The second Piola–Kirchhoff stress \mathbf{T} is the work conjugate of the Green strain \mathbf{E} , and is obtained from (9) as

$$\mathbf{T} = \frac{\partial U}{\partial \mathbf{E}} = J \frac{dU^V}{dJ} \bar{\mathbf{C}}^{-1} + \frac{2\sigma}{3\varepsilon} \left[J^{-\frac{2}{3}} \bar{\mathbf{E}} - \left(\varepsilon^2 + \frac{\bar{E}_{KK}}{3} \right) \bar{\mathbf{C}}^{-1} \right], \quad (10)$$

where $\bar{\mathbf{C}}$ is the reciprocal of the right Cauchy–Green strain tensor \mathbf{C} in (3), \bar{E}_{KK} is the first invariant of $\bar{\mathbf{E}}$, and $\sigma = \frac{dU^D}{d\varepsilon}$. The simplest form for U^V and U^D is

$$U^V = \frac{K}{2}(J-1)^2, \quad U^D = \frac{\sigma_{\text{ref}}}{N+1} \varepsilon^{N+1}, \quad (11)$$

which gives $\sigma = \frac{dU^D}{d\varepsilon} = \sigma_{\text{ref}} \varepsilon^N$, where K is the elastic bulk modulus, $N (< 1)$ is the work hardening exponent, and σ_{ref} is a reference stress in uniaxial tension. For infinitesimal deformation, (10) and (11) degenerate to the J_2 -deformation plasticity theory, $\boldsymbol{\sigma} = K \varepsilon_{kk} \mathbf{1} + \frac{2\sigma}{3\varepsilon} \boldsymbol{\varepsilon}'$, where $\boldsymbol{\varepsilon}'$ is the deviatoric strain.

3. The Taylor dislocation model

The Taylor (1938) model gives the shear flow stress τ in terms of the dislocation density ρ ,

$$\tau = \alpha \mu b \sqrt{\bar{\rho}} = \alpha \mu b \sqrt{\rho_S + \rho_G}, \quad (12)$$

where α is an empirical material constant between 0.1 and 0.5, μ is the shear modulus, b is the Burgers vector, and ρ_S and ρ_G are the densities of statistically stored and geometrically necessary dislocations, respectively. The density ρ_G of geometrically necessary dislocations is proportional to the effective strain gradient η (e.g. Ashby, 1970; Nix and Gao, 1998; Huang et al., 2000b), while the density ρ_S of statistically stored dislocations is related to the uniaxial stress-strain relation, which generally takes a power-law form $\sigma = \sigma_{\text{ref}} \varepsilon^N$ (Nix and Gao, 1998; Gao et al., 1999), where σ_{ref} is a reference stress and $N (< 1)$ is the plastic work hardening exponent. The tensile flow stress σ is obtained from (12) as (Nix and Gao, 1998; Gao et al., 1999; Huang et al., 2000b)

$$\sigma = \sigma_{\text{ref}} \sqrt{\varepsilon^{2N} + l\eta} = \sqrt{(\sigma_{\text{ref}} \varepsilon^N)^2 + 18\alpha^2 \mu^2 b \eta}, \quad (13)$$

where ε is the von Mises effective strain for infinitesimal deformation and is generalized to the effective strain in (8) for finite deformation; l is the intrinsic material length in strain gradient plasticity given by

$$l = 18\alpha^2 \left(\frac{\mu}{\sigma_{ref}} \right)^2 b, \tag{14}$$

which is indeed on the order of microns for typical metallic materials; via three dislocation models the effective strain gradient η has been determined in terms of deviatoric strain gradient (Gao et al., 1999), and it is generalized for finite deformation by

$$\eta = \frac{1}{2} \sqrt{\tilde{\eta}_{IJK} \tilde{\eta}_{IJK}} \tag{15}$$

Here $\tilde{\eta}_{IJK}$ is the strain gradient tensor excluding the volumetric deformation and is given in terms of the isochoric Green strain \tilde{E} in (5) by

$$\tilde{\eta}_{IJK} = \tilde{E}_{IK,J} + \tilde{E}_{JK,I} - \tilde{E}_{IJ,K}. \tag{16}$$

4. A finite deformation theory of mechanism-based strain gradient plasticity

Gao et al. (1999) adopted a multiscale, hierarchical framework to develop a mesoscale theory of mechanism-based strain gradient from the Taylor dislocation model on the microscale. The same framework, as shown in Fig. 1, is adopted in the present study in order to establish the corresponding finite deformation theory.

Stress and strain are defined in the classical sense on the microscale, and are denoted by \tilde{T} (second Piola–Kirchhoff stress) and \tilde{E} (Green strain), respectively, where tilde [$\tilde{\dots}$] denotes the microscale measure. Concepts associated with strain

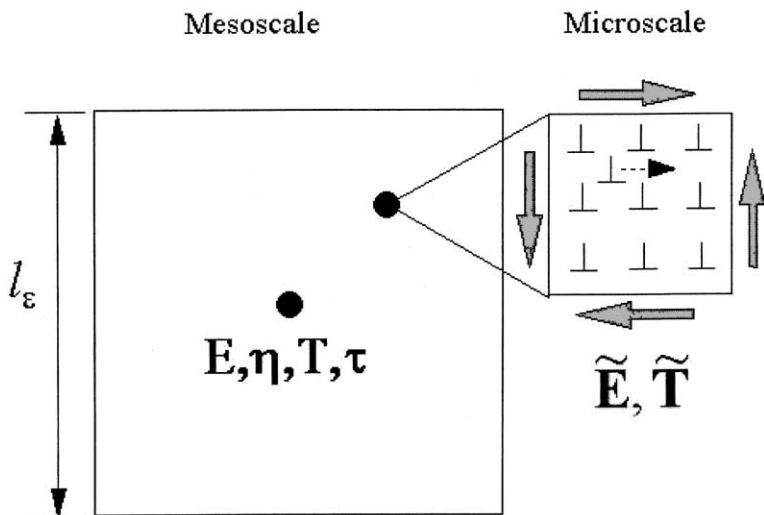


Fig 1. A schematic diagram of the multiscale framework to connect the mesoscale theory of strain gradient plasticity to the Taylor dislocation model on the microscale.

gradient plasticity are introduced on the mesoscale, such as the strain gradient tensor $\boldsymbol{\eta}$ and higher-order stress $\boldsymbol{\tau}$, where $\boldsymbol{\eta}$ is defined in terms of the mesoscale Green strain \mathbf{E} by

$$\eta_{IJK} = E_{IK,J} + E_{JK,I} - E_{IJ,K}, \tag{17}$$

and $\boldsymbol{\tau}$ is the work conjugate of $\boldsymbol{\eta}$. The microscale strain within the mesoscale cell (Fig. 1) is related to the mesoscale strain measures by the Taylor expansion,

$$\tilde{E}_{IJ} = E_{IJ} + E_{IJ,K}\tilde{X}_K + 0\left(|\tilde{X}|^2\right) = E_{IJ} + \frac{1}{2}(\eta_{KIJ} + \eta_{KJI})\tilde{X}_K + 0\left(|\tilde{X}|^2\right), \tag{18}$$

where \tilde{X}_K is the local coordinate originated at the center of the mesoscale cell.

4.1. Microscale analysis

The stress $\tilde{\mathbf{T}}$ and strain $\tilde{\mathbf{E}}$ on the microscale satisfy the constitutive relation (10) except the stress $\tilde{\sigma}$, which is governed by the Taylor dislocation model in (13),

$$\tilde{\sigma} = \sigma_{\text{ref}}\sqrt{\tilde{\varepsilon}^{2N} + l\eta}, \tag{19}$$

where the microscale effective strain $\tilde{\varepsilon}$ is related to the microscale Green strain $\tilde{\mathbf{E}}$ in the same way as in (8), and η is the mesoscale effective strain gradient given in (15).

The microscale constitutive relation now becomes

$$\tilde{\mathbf{T}} = \tilde{J} \frac{dU^V(\tilde{J})}{d\tilde{J}} \tilde{\mathbf{C}}^{-1} + \frac{2\tilde{\sigma}}{3\tilde{\varepsilon}} \left[\tilde{J}^{-\frac{2}{3}} \tilde{\mathbf{E}} - \left(\tilde{\varepsilon}^2 + \frac{\tilde{E}_{KK}}{3} \right) \tilde{\mathbf{C}}^{-1} \right] \tag{20}$$

where the microscale variables can be expressed in terms of the mesoscale ones via Taylor expansion up to the first order, such as

$$\tilde{J} = J + \frac{dJ}{dX_K} \tilde{X}_K = J + JC_{MN}^{-1} \eta_{KMN} \tilde{X}_K, \tag{21}$$

$$\tilde{\mathbf{C}}_{IJ}^{-1} = \mathbf{C}_{IJ}^{-1} - \mathbf{C}_{IM}^{-1} \mathbf{C}_{JN}^{-1} (\eta_{KMN} + \eta_{KNM}) \tilde{X}_K, \tag{22}$$

$$\tilde{E}_{IJ} = E_{IJ} + \frac{1}{2}(\bar{\eta}_{KIJ} + \bar{\eta}_{KJI}) \tilde{X}_K. \tag{23}$$

4.2. Mesoscale analysis

The mesoscale constitutive relations are derived from the work equality between the micro- and mesoscales,

$$\int_{V_{\text{cell}}} \tilde{T}_{IJ} \delta \tilde{E}_{IJ} dV = (T_{IJ} \delta E_{IJ} + \tau_{IJK} \delta \eta_{IJK}) V_{\text{cell}}, \tag{24}$$

where the integration is over the mesoscale cell V_{cell} in the reference configuration (Fig. 1), and δ stands for the virtual variation. Using the kinematics relation (18) between the strain measures on these two scales, we obtain the mesoscale stress T_{IJ} and higher-order stress τ_{IJK} in terms of microscale stress \tilde{T}_{IJ} ,

$$T_{IJ} = \frac{1}{V_{\text{cell}}} \int_{V_{\text{cell}}} \tilde{T}_{IJ} dV, \tag{25}$$

$$\tau_{IJK} = \frac{1}{2V_{\text{cell}}} \int_{V_{\text{cell}}} \left(\tilde{T}_{KI} \tilde{X}_J + \tilde{T}_{KJ} \tilde{X}_I \right) dV \tag{26}$$

Substituting the microscale constitutive relation (20) into (25) and (26), we obtain the following finite deformation mesoscale constitutive relations for MSG plasticity,

$$T_{IJ} = KJ(J - 1) \bar{C}_{IJ}^{-1} + \frac{2\sigma}{3\varepsilon} \left[J^{-\frac{2}{3}} \bar{E}_{IJ} - \left(\varepsilon^2 + \frac{\bar{E}_{KK}}{3} \right) \bar{C}_{IJ}^{-1} \right], \tag{27}$$

$$\tau_{IJK} + l_\varepsilon^2 \left\{ \frac{K}{6} V_{IJK} + \frac{\sigma}{\varepsilon} \Lambda_{IJK} + \left[\frac{\sigma_{\text{ref}}^2}{\sigma} f(\varepsilon) f'(\varepsilon) - \frac{\sigma}{\varepsilon} \right] \Pi_{IJK} \right\}, \tag{28}$$

where σ is given in (13), $l_\varepsilon = 10 \frac{\mu}{\sigma_Y} b$ and is less than 100 nm for typical metallic materials (Gao et al., 1999; Huang et al., 2000a,b), σ_Y is the initial yield stress,

$$V_{IJK} = \frac{1}{4} J \left\{ (2J - 1) \bar{C}_{MN}^{-1} \left(\bar{C}_{JK}^{-1} \eta_{IMN} + \bar{C}_{IK}^{-1} \eta_{JMN} \right) - (J - 1) \left[\bar{C}_{JM}^{-1} \bar{C}_{KN}^{-1} (\eta_{IMN} + \eta_{INM}) + \bar{C}_{IM}^{-1} \bar{C}_{KN}^{-1} (\eta_{JMN} + \eta_{JNM}) \right] \right\}, \tag{29}$$

$$\begin{aligned} \Lambda_{IJK} = & \frac{1}{72} \left[-\frac{4}{3} J^{\frac{4}{3}} \bar{C}_{MN}^{-1} (\eta_{IMN} C_{JK} + \eta_{IMN} C_{IK}) + J^{-\frac{4}{3}} (2\eta_{IJK} + \eta_{IKJ} + \eta_{JKI}) \right. \\ & + \frac{2}{3} J^{\frac{2}{3}} \bar{C}_{MN}^{-1} (\eta_{IMN} \delta_{JK} + \eta_{IMN} \delta_{IK}) - J^{\frac{2}{3}} \bar{E}_{MN} \left(\bar{\eta}_{IMN} \bar{C}_{JK}^{-1} + \bar{\eta}_{JMN} \bar{C}_{IK}^{-1} \right) \\ & - \frac{2}{3} \bar{\eta}_{IPP} \bar{C}_{JK}^{-1} - \frac{2}{3} \bar{\eta}_{JPP} \bar{C}_{IK}^{-1} + 2 \left(\varepsilon^2 + \frac{\bar{E}_{PP}}{3} \right) \bar{C}_{JM}^{-1} \bar{C}_{KN}^{-1} (\eta_{IMN} + \eta_{INM}) \\ & \left. + 2 \left(\varepsilon^2 + \frac{\bar{E}_{PP}}{3} \right) \bar{C}_{IM}^{-1} \bar{C}_{KN}^{-1} (\eta_{JMN} + \eta_{JNM}) \right], \end{aligned} \tag{30}$$

$$\begin{aligned} \Pi_{IJK} = & \frac{\bar{E}_{MN}}{54\varepsilon^2} \left\{ \bar{\eta}_{IMN} \left[J^{-\frac{2}{3}} \bar{E}_{JK} - \left(\varepsilon^2 + \frac{\bar{E}_{PP}}{3} \right)^{-1} \bar{C}_{JK} \right] \right. \\ & \left. + \eta_{JMN} \left[J^{-\frac{2}{3}} \bar{E}_{IK} - \left(\varepsilon^2 + \frac{\bar{E}_{PP}}{3} \right)^{-1} \bar{C}_{IK} \right] \right\}. \end{aligned} \tag{31}$$

The above constitutive relations degenerate to Gao et al. (1999) and Huang et al. (2000b) for infinitesimal deformation.

Based on the principle of virtual work, Hwang et al. (2001) derived the equilibrium equations and traction boundary conditions in terms of the second Piola–Kirchhoff stress and the higher-order stress. These equilibrium equations and traction boundary conditions hold for finite deformation strain gradient theories, regardless of the constitutive law.

5. Analytical and numerical studies

5.1. Torsion of a thin cylinder

We investigate the torsion of a thin cylinder in this section. The cylinder has a circular cross section with an initial thickness h and mean radius R_0 , where R_0 is on the order of microns or larger. For each material point, the cylindrical coordinates in the reference (undeformed) and current (deformed) configurations are (R, Θ, Z) and (r, θ, z) , respectively, and they are related by (Fig. 2)

$$r = r(R), \quad \theta = \Theta + \kappa Z, \quad z = (1 + \beta)Z, \tag{32}$$

where κ is the twist (angle of rotation per unit length in the axial direction), β is the nominal axial strain to be determined due to finite deformation effect, and the function $r(R)$ is also to be determined. The displacement is

$$u = r e_r + z e_z - (R e_R + Z e_z), \tag{33}$$

where (e_r, e_θ, e_z) and (e_R, e_Θ, e_z) are the unit vectors along the radial, circumferential and axial directions in the current and reference configurations, respectively, and they are related by

$$e_r = \cos \kappa Z e_R + \sin \kappa Z e_\Theta, \quad e_\theta = -\sin \kappa Z e_R + \cos \kappa Z e_\Theta, \quad e_z = e_z. \tag{34}$$

The deformation gradient \mathbf{F} is obtained from (33) as

$$\mathbf{F} = \frac{dr}{dR} e_r e_R + \frac{r}{R} e_\theta e_R + \frac{r}{R} e_\theta e_\Theta + \kappa r e_\theta e_z + (1 + \beta) e_z e_z, \tag{35}$$

which has the determinant

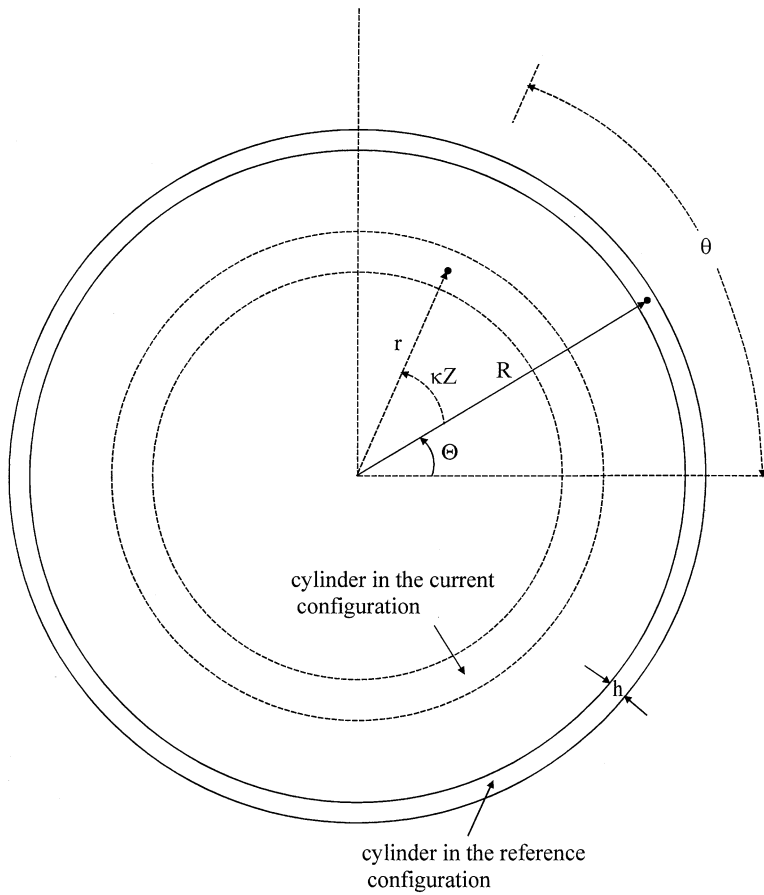


Fig 2. The cross section of a thin tube under torsion, where (r, θ, z) and (R, Θ, Z) denote the cylindrical coordinates in the current and reference configurations, respectively; κ is the twist (angle of rotation per unit length in the axial direction).

$$J = \det(\mathbf{F}) = \frac{dr}{dR} \frac{r}{R} (1 + \beta). \tag{36}$$

The right Cauchy–Green strain tensor \mathbf{C} in the reference configuration is obtained from (3)₁ as

$$\mathbf{C} = \begin{pmatrix} \left(\frac{dr}{dR}\right)^2 & 0 & 0 \\ 0 & \frac{r^2}{R^2} & \frac{\kappa r^2}{R} \\ 0 & \frac{\kappa r^2}{R} & \kappa^2 r^2 + (1 + \beta^2) \end{pmatrix}. \tag{37}$$

The Green strain tensor \mathbf{E} and isochoric Green strain tensor $\tilde{\mathbf{E}}$ can be obtained similarly from (3)₃ and (5)₃.

For a thin cylinder with the thickness h much less than the mean radius R_0 , the Taylor expansion of radial coordinate r in the current configuration gives

$$r = r_0 + \left(\frac{dr}{dR}\right)_0 (R - R_0) + O[(R - R_0)^2], \tag{38}$$

where the subscript 0 denotes the variables at the center of cylinder wall. The right Cauchy–Green strain tensor \mathbf{C} in (37) can also be evaluated at the center of cylinder wall to give the non-vanishing components as

$$\begin{aligned} C_{RR} &= \left(\frac{dr}{dR}\right)_0^2, \quad C_{\Theta\Theta} = \left(\frac{r_0}{R_0}\right)^2, \quad C_{\Theta Z} = C_{Z\Theta} = \frac{kr_0^2}{R_0}, \\ C_{ZZ} &= k^2 r_0^2 + (1 + B)^2. \end{aligned} \tag{39}$$

Similarly, the determinant of \mathbf{F} in (36) becomes $J = \left(\frac{dr}{dR}\right)_0 \frac{r_0}{R_0} (1 + \beta)$, and the non-vanishing components of the isochoric Green strain tensor $\tilde{\mathbf{E}}$ in (5)₃ are

$$\begin{aligned} \tilde{E}_{RR} &= \frac{1}{2} \left[J^{-\frac{2}{3}} \left(\frac{dr}{dR}\right)_0^2 - 1 \right], \quad \tilde{E}_{\Theta\Theta} = \frac{1}{2} \left[J^{-\frac{2}{3}} \left(\frac{r_0}{R_0}\right)^2 - 1 \right], \\ \tilde{E}_{\Theta Z} &= \tilde{E}_{Z\Theta} = J^{-\frac{2}{3}} \frac{kr_0^2}{2R_0}, \quad \tilde{E}_{ZZ} = \frac{1}{2} \left\{ J^{-\frac{2}{3}} [k^2 r_0^2 + (1 + \beta^2)] - 1 \right\}. \end{aligned} \tag{40}$$

The isochoric strain gradient tensor $\bar{\boldsymbol{\eta}}$ in (16) can be written as

$$\bar{\boldsymbol{\eta}} = \frac{1}{3r_0 J^{\frac{2}{3}}} \boldsymbol{\zeta}, \tag{41}$$

where the non-vanishing components are

$$\begin{aligned} \zeta_{RRR} &= -\left(\frac{dr}{dR}\right)_0^2 \Delta, \quad \zeta_{R\Theta\Theta} = \zeta_{\Theta R\Theta} = 2 \frac{r_0^2}{R_0^2} \Delta, \\ \zeta_{R\Theta Z} &= \zeta_{\Theta RZ} = 2 \frac{kr_0^2}{R_0} \Delta, \quad \zeta_{\Theta\Theta R} = \frac{r_0}{R_0} \left(4 \frac{r_0}{R_0} + 3\Delta \right) \Delta, \\ \zeta_{RZ\Theta} &= \zeta_{ZR\Theta} = \zeta_{\Theta ZR} = -\zeta_{Z\Theta R} = \frac{kr_0^2}{R_0} \left(3 \frac{r_0}{R_0} + 2\Delta \right) \\ \zeta_{RZZ} &= \zeta_{ZRZ} = -\zeta_{ZZR} = -[k^2 r_0^2 + (1 + \beta^2)] \Delta + 3k^2 r_0^2 \left(\frac{dr}{dR}\right)_0, \end{aligned} \tag{42}$$

and $\Delta = \left(\frac{dr}{dR}\right)_0 - \frac{r_0}{R_0}$. The effective strain and effective strain gradient are then obtained by substituting (40)–(42) into (8) and (15), respectively. For a given twist κ and

cylinder radius R_0 , the above strains and strain gradients involve three parameters to be determined, namely r_0 , $\left(\frac{dr}{dR}\right)_0$ and β .

The constitutive law (27) gives the non-vanishing components of the second Piola–Kirchhoff stress as

$$\begin{aligned} T_{RR} &= \frac{\sigma}{3\varepsilon} \left[J^{-\frac{4}{3}} C_{RR} - J^{-\frac{2}{3}} - 2 \left(\varepsilon^2 + \frac{\bar{E}_{KK}}{3} \right) \bar{C}_{RR}^{-1} \right] + KJ(J-1) \bar{C}_{RR}^{-1}, \\ T_{\Theta\Theta} &= \frac{\sigma}{3\varepsilon} \left[J^{-\frac{4}{3}} C_{\Theta\Theta} - J^{-\frac{2}{3}} - 2 \left(\varepsilon^2 + \frac{\bar{E}_{KK}}{3} \right) \bar{C}_{\Theta\Theta}^{-1} \right] + KJ(J-1) \bar{C}_{\Theta\Theta}^{-1}, \\ T_{\Theta Z} &= T_{Z\Theta} = \frac{\sigma}{3\varepsilon} \left[J^{-\frac{4}{3}} C_{\Theta Z} - 2 \left(\varepsilon^2 + \frac{\bar{E}_{KK}}{3} \right) \bar{C}_{\Theta Z}^{-1} \right] + KJ(J-1) \bar{C}_{\Theta Z}^{-1}, \\ T_{ZZ} &= \frac{\sigma}{3\varepsilon} \left[J^{-\frac{4}{3}} C_{ZZ} - J^{-\frac{2}{3}} - 2 \left(\varepsilon^2 + \frac{\bar{E}_{KK}}{3} \right) \bar{C}_{ZZ}^{-1} \right] + KJ(J-1) \bar{C}_{ZZ}^{-1}. \end{aligned} \quad (43)$$

The higher-order stress can be obtained similarly from (28). The substitution of stress in (43) and higher-order stress into the equilibrium equations (Hwang et al., 2001) leads to three ordinary differential equations involving a nondimensional parameter $\left(\frac{l_e}{R_0}\right)^2$, which is less 1% since R_0 is larger than microns and l_e is less than 100 nm. Accordingly, we neglect the terms on the order of $\left(\frac{l_e}{R_0}\right)^2$ as compared to unity. This is consistent with the prior studies that suggest l_e has essentially no effect on macroscopic quantities (Huang et al., 2000a,b). In conjunction with the traction boundary conditions, the equilibrium equations can be integrated to give three algebraic equations

$$T_{RR} = 0, \quad (44)$$

$$T_{\Theta\Theta} + 2kR_0 T_{\Theta Z} = 0, \quad (45)$$

$$T_{ZZ} = 0, \quad (46)$$

which are solved numerically to determine three unknown parameters, r_0 , $\left(\frac{dr}{dR}\right)_0$ and β for each given twist κ .

The Cauchy (true) stress σ can be obtained from the second Piola–Kirchhoff stress by

$$\sigma = \frac{1}{J} \mathbf{F} \cdot \mathbf{T} \cdot \mathbf{F}^T = \left(\frac{dr}{dR} \right)_0^{-1} T_{\Theta Z} (e_\theta e_z + e_z e_\theta), \quad (47)$$

where the deformation gradient in (35) has been used. The Cauchy stress has only the shear component along the circumferential direction in the current configuration. In fact, it can be shown from $\sigma_{kk} = 0$ that there is no volumetric deformation in the finite twist of a thin cylinder, i.e. $J = 1$. The applied torque can be found from

(47) as

$$T = 2\pi r_0^2 h T_{\Theta Z}, \tag{48}$$

where h is the initial thickness of the cylinder and r_0 is the mean cylinder radius in the current configuration.

Fig 3 shows the normalized torque, $T/(2\pi R_0^2 h \sigma_Y)$, versus the normalized twist, κR_0 , for $l/R_0 = 1, 0.5, 0.1$ and 0 , where R_0 and h are the initial mean cylinder radius and thickness in the reference configuration, l is the intrinsic material length in (14), the initial yield stress σ_Y is 0.2% times the Young’s modulus E , and $l/R_0 = 0$ corresponds to classical plasticity theory (without strain gradient effect). Other material properties include the Poisson’s ratio $\nu = 0.3$, plastic work hardening exponent $N = 0.2$, and the reference stress $\sigma_{ref} = \sigma_Y \left(\frac{E}{\sigma_Y}\right)^N$. The empirical material constant α in the Taylor dislocation model and the Burgers vector b only appear through the intrinsic material length l in (14), and it is therefore not necessary to specify the values of α and b for a given ratio l/R_0 . For a small twist, $\kappa R_0 < 0.1$, there is little or no strain gradient effect since all curves are essentially the same. This is because the strain gradient term $18\alpha^2 \mu^2 b \eta$ is much less than $(\sigma_{ref} \varepsilon^N)^2$ in the flow stress (13) for a small twist of the thin cylinder. As the deformation increases, the strain gradient

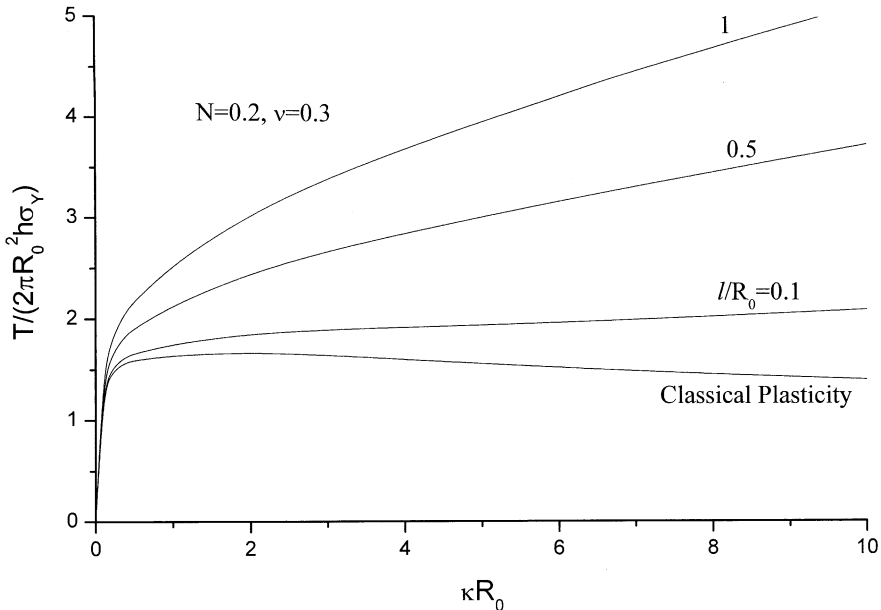


Fig 3. The normalized torque, $T/(2\pi R_0^2 h \sigma_Y)$, versus the normalized twist, κR_0 , for several ratios of intrinsic material length to mean radius of the cylinder, l/R_0 , where h and R_0 are the thickness and mean radius of the cylinder in the reference configuration, respectively; σ_Y is the initial yield stress, and l is the intrinsic material length for MSG plasticity. The limit $l/R_0 = 0$ corresponds to classical plasticity. Plasticity work hardening exponent $N = 0.2$, Young’s modulus $E = 500\sigma_Y$, and Poisson’s ratio $\nu = 0.3$.

effect becomes significant. For example, the classical plasticity theory ($l/R_0 = 0$) predicts a maximum torque that occurs approximately at $\kappa R_0 = 0.5$, but there is no maximum torque for MSG plasticity ($l/R_0 \geq 0$). The curves for cylinder radius being one or two times the intrinsic material length l (i.e. $l/R_0 = 1, 0.5$) are much higher than that predicted by classical plasticity, which is clearly due to the strain gradient effect. Even the curve for cylinder radius being ten times l (i.e. $\frac{l}{R_0} = 0.1$) shows significant size effect.

Fig 4 shows the torque-twist relation for both infinitesimal and finite deformation theories of classical plasticity ($l/R_0 = 0$) and MSG plasticity ($l/R_0 = 1$). The material properties and the normalizations are identical to those in Fig. 3. The curves accounting for finite deformation are significantly lower than those for infinitesimal deformation, indicating the finite deformation effect is significant for $\kappa R_0 > 0.1$.

5.2. Mode-I fracture analysis

Jiang et al. (2001) used the infinitesimal deformation MSG plasticity theory (Gao et al., 1999; Huang et al., 2000a,b) to investigate fracture around a stationary mode-I crack tip field. Due to the strain gradient effect, stress level around the crack tip in MSG plasticity is significantly higher than that in the classical plasticity, i.e. the

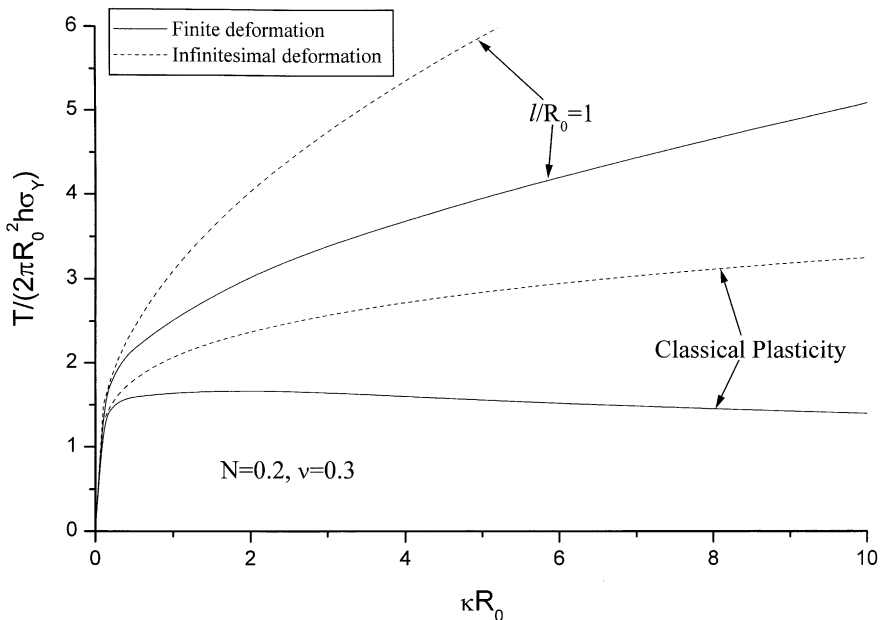


Fig. 4. The normalized torque, $T/(2\pi R_0^2 h \sigma_Y)$, versus the normalized twist, κR_0 , for both finite and infinitesimal deformation theories of MSG plasticity ($l/R_0 = 1$) and classical plasticity ($l/R_0 = 0$), where h and R_0 are the thickness and mean radius of the cylinder in the reference configuration, respectively; σ_Y is the initial yield stress, l is the intrinsic material length for MSG plasticity. Plasticity work hardening exponent $N = 0.2$, Young's modulus $E = 500\sigma_Y$, and Poisson's ratio $\nu = 0.3$.

HRR field (Hutchinson, 1968; Rice and Rosengren, 1968). The numerical results also showed that the stress around the crack tip in MSG plasticity is not only more singular than the HRR field, but also more singular than the classical elastic K field (square-root singularity). This provides a means to explain the cleavage fracture observed in ductile materials (e.g. Elssner et al., 1994).

We use the same loading, material properties, and finite element mesh as Jiang et al. (2001) but the finite deformation effect is accounted for. We take a circular domain of radius 10^3l centered at the crack tip in our plane-strain finite element analysis, where l is the intrinsic material length in (14). The origin of the coordinate system coincides with the crack tip, while the traction-free crack faces coincide with the negative x_1 axis. The classical mode-I elastic K field is imposed on the outer boundary of the domain (10^3l) with the elastic stress intensity K_I increasing monotonically.

The stress intensity factor K_I is normalized by $\sigma_Y l^{1/2}$ in the numerical analysis, where $\sigma_Y = 0.2\% E$ is the initial yield stress, E is the Young's modulus, and l is the intrinsic material length in (14). The stress is normalized by σ_Y , while the position (coordinate) is normalized by l . Other material properties include the plastic work hardening exponent $N = 0.2$, Poisson's ratio $\nu = 0.3$, and the reference stress in (13). The empirical material constant α in the Taylor dislocation model and the Burgers vector b only appear through the intrinsic material length l in (14), and it is therefore not necessary to specify the values of α and b for the above normalizations.

Fig 5 shows the distribution of the normalized stress ahead of the mode-I crack tip, i.e. $\sigma_{\theta\theta}/\sigma_Y$, versus the normalized distance r/l to the crack tip, where $\sigma_{\theta\theta}$ is the Cauchy (true) stress along $\theta = 1.014^\circ$ ($\theta = \pm 180^\circ$ being the crack faces), and r is the distance to the crack tip in the reference (undeformed) configuration. The remote applied stress intensity factor is $K_I = 10\sigma_Y l^{1/2}$. The distribution of $\sigma_{\theta\theta}$ for infinitesimal deformation MSG plasticity theory (Jiang et al., 2001) and the corresponding curves for classical plasticity (i.e. without the strain gradient effect) are also shown for comparison. For $r > 10l$, all curves become the same straight line with the slope of $-1/2$, corresponding to the elastic K_I field (since the slope represents the order of singularity in the log–log plot). For r between $0.3l$ and $10l$, all curves still coincide but they deviate significantly from the straight line (of the slope $-1/2$). This indicates that the material undergoes significant plastic deformation, though neither the strain gradient effect nor the finite deformation effect is important in this range. Once the distance r to the crack tip is less than $0.3l$, the normal stresses $\sigma_{\theta\theta}$ predicted by MSG plasticity (for both finite and infinitesimal deformation) increase much quicker than their counterparts in classical plasticity. A representative value of the intrinsic material length is $l = 5 \mu\text{m}$ [Fleck et al., 1994; Stolken and Evans, 1998; Eq. (14) with $\alpha = 0.5$ and $b = 0.3\text{nm}$]. At a distance $r = 0.02l = 0.1 \mu\text{m}$ to the crack tip, which is still within the intended range of applications for MSG plasticity (Gao et al., 1999; Huang et al., 2000b), the normal stress $\sigma_{\theta\theta}$ predicted by MSG plasticity is approximately twice of that for classical plasticity. For infinitesimal deformation theories, the curve for classical plasticity has the slope of $-N/(N+1)$ and corresponds to the HRR field (Hutchinson, 1968; Rice and Rosengren, 1968), while the curve for MSG plasticity has the slope higher than $1/2$ (in absolute value), indicating the crack tip field in MSG plasticity is more singular than not only the HRR field,

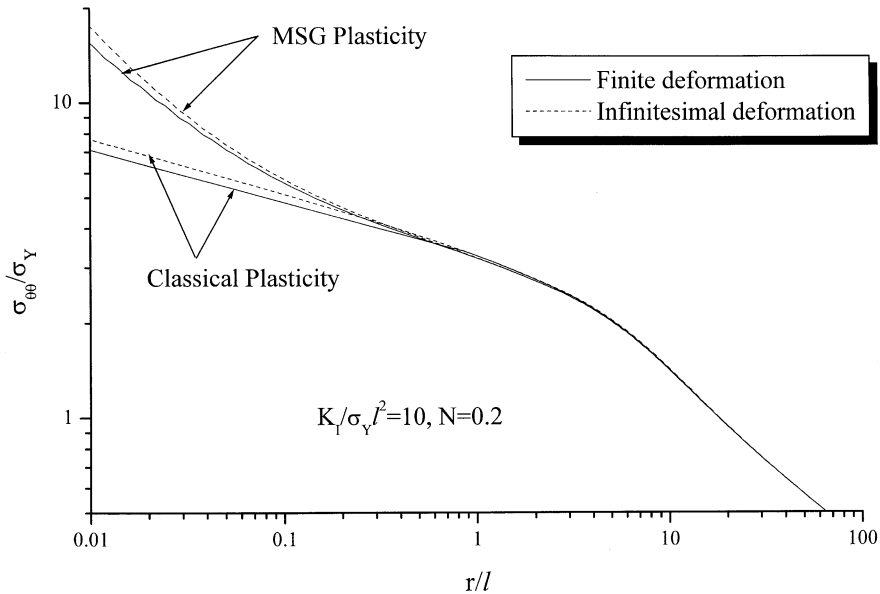


Fig. 5. The Cauchy (true) stress $\sigma_{\theta\theta}$ normalized by the initial yield stress σ_Y versus the normalized distance to the crack tip, r/l , ahead of the crack tip (polar angle $\theta = 1.014^\circ$), where l is the intrinsic material length for MSG plasticity, the plastic work hardening exponent $N = 0.2$, Poisson's ratio $\nu = 0.3$, the ratio of yield stress to elastic modulus $\sigma_Y/E = 0.2\%$, and the remotely applied elastic stress intensity factor $K_I/\sigma_Y l^{1/2} = 10$. The results are presented for both finite and infinitesimal deformation of MSG plasticity and classical plasticity.

but also the classical elastic K field. The effect of finite deformation does not seem to be significant in Fig. 5, as seen from the comparison between curves for infinitesimal and finite deformation. This is because we have taken a relatively small applied stress intensity factor ($K_I = 10\sigma_Y l^{1/2}$). In fact, the strain is only a few percent ($\sim 3\%$) at a distance of $0.1 \mu\text{m}$ ($r = 0.02l$) to the crack tip. It can be established from Fig. 4 that the strain level needs to be significantly higher ($> 10\%$) in order to display the difference between the finite and infinitesimal deformation. We have indeed imposed a much larger applied stress intensity factor, but the finite deformation analysis has some numerical difficulties in convergence.

6. Summary

We have developed a finite deformation theory of mechanism-based strain gradient (MSG) plasticity based on the Taylor dislocation model. The theory ensures the proper decomposition of deformation into volumetric and deviatoric parts such that the volumetric deformation does not contribute to the deviatoric strain gradient, which represents the density of geometrically necessary dislocations. We have conducted the analytic study for a thin cylinder under large torsion, and established that the effect of finite deformation is significant when $\kappa R_0 > 0.1$, where κ is the twist

and R_0 is the initial mean radius of the cylinder. We have also used the finite element method to investigate mode-I fracture in MSG plasticity, and established that the crack tip field in MSG plasticity has a much higher stress level than its counterpart, i.e. the HRR field in classical plasticity.

Acknowledgements

K.C.H. acknowledges the support from the Ministry of Education, China. Y.H. acknowledges NSF (grant CMS-0084980 and a supplement to grant CMS-9896285 from NSF International Program). H.G. acknowledges NSF (grant CMS-9979717). The authors also acknowledge the support from NSFC.

References

- Acharya, A., Bassani, J.L., 2000. Lattice incompatibility and a gradient theory of crystal plasticity. *J. Mech. Phys. Solids* 48, 1565–1595.
- Acharya, A., Beaudoin, A.J., 2000. Grain-size effect in viscoplastic polycrystals at moderate strains. *J. Mech. Phys. Solids* 48, 2213–2230.
- Aifantis, E.C., 1984. On the microstructural origin of certain inelastic models. *J. Eng. Mater. Tech.* 106, 326–330.
- Aifantis, E.C., 1992. On the role of gradients in the localization of deformation and fracture. *Int. J. Eng. Sci.* 30, 1279–1299.
- Arsenlis, A., Parks, D.M., 1999. Crystallographic aspects of geometrically-necessary and statistically-stored dislocation density. *Acta Mater.* 47, 1597–1611.
- Ashby, M.F., 1970. The deformation of plastically non-homogeneous alloys. *Phil. Mag.* 21, 399–424.
- Chen, S.H., Wang, T.C., 2000. A new hardening law for strain gradient plasticity. *Acta Mater.* 48, 3997–4005.
- Cleveringa, H.H.M., Van Der Giessen, E., Needleman, A., 1997. Comparison of discrete dislocation and continuum plasticity predictions for a composite material. *Acta Mater.* 45, 3163–3179.
- Cleveringa, H.H.M., Van Der Giessen, E., Needleman, A., 1998. Discrete dislocation simulations and size dependent hardening in single slip. *J. de Physique IV* 8, 83–92.
- Cleveringa, H.H.M., Van Der Giessen, E., Needleman, A., 1999a. Discrete dislocation analysis of bending. *Int. J. Plasticity* 15, 837–868.
- Cleveringa, H.H.M., Van Der Giessen, E., Needleman, A., 1999b. A discrete dislocation analysis of residual stresses in a composite material. *Phil. Mag. A* 79, 893–920.
- Cleveringa, H.H.M., Van Der Giessen, E., Needleman, A., 2000. Discrete dislocation analysis of mode I crack growth. *J. Mech. Phys. Solids* 48, 1133–1157.
- Cottrell, A.H., 1964. *The Mechanical Properties of Matter*. Wiley, New York. p. 277.
- Dai, H., Parks, D.M., 2001. Geometrically necessary dislocation density in continuum crystal plasticity theory and FEM implementation (unpublished manuscript).
- de Borst, R., Mühlhaus, H.-B., 1991. Computational strategies for gradient continuum models with a view to localization of deformation. In: Bicanic, N., Marovic, P., Owen, D.R.J., Jovic, V., Mihanovic, A. (Eds.), *Proc Int Conf Nonlinear Eng. Comp.* Prineridge Press, Swansea, pp. 239–260.
- de Borst, R., Mühlhaus, H.-B., 1992. Gradient-dependent plasticity: formulation and algorithmic aspects. *Int. J. Numer. Met. Eng.* 35, 521–539.
- Ellsner, G., Korn, D., Rühle, M., 1994. The influence of interface impurities on fracture energy of UHV diffusion bonded metal-ceramic bicrystals. *Scripta Metall Mater.* 31, 1037–1042.
- Fleck, N.A., Hutchinson, J.W., 1993. A phenomenological theory for strain gradient effects in plasticity. *J. Mech. Phys. Solids* 41, 1825–1857.

- Fleck, N.A., Hutchinson, J.W., 1997. Strain gradient plasticity. In: Hutchinson, J.W., Wu, T.Y. (Eds.), *Advances in Applied Mechanics*, Vol. 33. Academic Press, New York, pp. 295–361.
- Fleck, N.A., Muller, G.M., Ashby, M.F., Hutchinson, J.W., 1994. Strain gradient plasticity: theory and experiments. *Acta Metall Mater.* 42, 475–487.
- Gao, H., Huang, Y., Nix, W.D., Hutchinson, J.W., 1999. Mechanism-based strain gradient plasticity—I. Theory. *J Mech. Phys. Solids* 47, 1239–1263.
- Gurtin, M.E., 2000. On the plasticity of single crystals: free energy, microforces, plastic-strain gradients. *J. Mech. Phys. Solids* 48, 989–1036.
- Gurtin, M.E., 2001. On a framework for small-deformation viscoplasticity: free energy, microforces, strain gradients. *Int. J. Plasticity* (in press).
- Huang, Y., Gao, H., Nix, W.D., Hutchinson, J.W., 2000a. Mechanism-based strain gradient plasticity—II. Analysis. *J Mech. Phys. Solids* 48, 99–128.
- Huang, Y., Xue, Z., Gao, H., Nix, W.D., Xia, Z.C., 2000b. A study of micro-indentation hardness tests by mechanism-based strain gradient plasticity. *J. Mater Res.* 15, 1786–1796.
- Hutchinson, J.W., 1968. Singular behavior at the end of a tensile crack in a hardening material. *J. Mech. Phys. Solids* 16, 13–31.
- Hwang, K.C., Jiang, H., Huang, Y., Gao, H., Hu, N., in press. A finite deformation theory of strain gradient plasticity. *J Mech. Phys. Solids*.
- Jiang, H., Huang, Y., Zhuang, Z., Hwang, K.C., 2001. Fracture in mechanism-based strain gradient plasticity. *J. Mech. Phys. Solids* 49, 979–993.
- Lasry, D., Belytschko, T., 1988. Localization limiters in transient problems. *Int. J. Solids Struct.* 24, 581–597.
- Lloyd, D.J., 1994. Particle reinforced aluminum and magnesium matrix composites. *Int. Mater Rev.* 39, 1–23.
- McElhaney, K.W., Vlassak, J.J., Nix, W.D., 1998. Determination of indenter tip geometry and indentation contact area for depth-sensing indentation experiments. *J. Mater Res.* 13, 1300–1306.
- Meissonnier, F.T., Busso, E.P., O'Dowd, N.P., 2001. Finite element implementation of a generalised non-local rate-dependent crystallographic formulation for finite strains. *Int. J. Plasticity* 17, 601–640.
- Muhlhaus, H.-B., Aifantis, E.C., 1991. A variational principle for gradient plasticity. *Int. J. Solids Struct.* 28, 845–857.
- Needleman, A., 2000. Computational mechanics at the mesoscale. *Acta Mater.* 48, 105–124.
- Nilsson, C., 1998. On nonlocal rate-independent plasticity. *Int. J. Plasticity* 14, 551–575.
- Nix, W.D., Gao, H., 1998. Indentation size effects in crystalline materials: a law for strain gradient plasticity. *J. Mech. Phys. Solids* 46, 411–425.
- Nye, J.F., 1953. Some geometrical relations in dislocated crystal. *Acta Metall* 1, 153–162.
- Rice, J.R., Rosengren, G.F., 1968. Plane strain deformation near a crack tip in a power law hardening material. *J. Mech. Phys. Solids* 16, 1–12.
- Shizawa, K., Zbib, H.M., 1999. A thermodynamical theory of gradient elastoplasticity with dislocation density tensor: I—fundamentals. *Int. J. Plasticity* 15, 899–938.
- Shu, J.Y., 1998. Scale-dependent deformation of porous single crystals. *Int. J. Plasticity* 14, 1085–1107.
- Shu, J.Y., Barlow, C.Y., 2000. Strain gradient effects on microscopic strain field in a metal matrix composite. *Int. J. Plasticity* 16, 563–591.
- Shu, J.Y., Fleck, N.A., 1999. Strain gradient crystal plasticity: size-dependent deformation of bicrystals. *J. Mech. Phys. Solids* 47, 292–324.
- Sluys, L.J., de Borst, R., Muhlhaus, H.-B., 1993. Wave propagation, localization, and dispersion in a gradient-dependent medium. *Int. J. Solids Struct.* 30, 1153–1171.
- Stolken, J.S., Evans, A.G., 1998. A microbend test method for measuring the plasticity length scale. *Acta Mater.* 46, 5109–5115.
- Taylor, G.I., 1938. Plastic strain in metal. *J. Inst Metals* 62, 307–324.
- Zbib, H.M., Aifantis, E.C., 1988. On the localization and postlocalization behavior of plastic deformation. Part I. On the initiation of shear bands; Part II. On the evolution and thickness of shear bands; Part III. On the structure and velocity of Portevin-Le Chatelier bands. *Res Mech.* 23, 261–277. 279–292, 293–305.
- Zbib, H.M., de la Rubia, T.D., in press. A multiscale model of plasticity. *Int. J. Plasticity*.